The Meteoritical Society

Meteoritics & Planetary Science 54, Nr 11, 2698–2709 (2019)
doi: 10.1111/maps.13381

A TEM and EELS study of carbon in a melt fragment from the Gardnos impact structure

Paula LINDGREN[1*], Lydia HALLIS[2], Fredrik S. HAGE[3], Martin R. LEE[2], John PARNELL[4], Anders PLAN[1], Alistair DOYE[5], and Ian MACLAREN[5]

[1]Department of Geology, Lund University, Sölvegatan 12, 223 62 Lund, Sweden
[2]School of Geographical & Earth Sciences, University of Glasgow, Glasgow G12 8QQ, UK
[3]SuperSTEM Laboratory, SciTech Daresbury Campus, Daresbury WA4 4AD, UK
[4]School of Geosciences, University of Aberdeen, Aberdeen AB24 3UE, UK
[5]School of Physics & Astronomy, University of Glasgow, Glasgow G12 8QQ, UK
[*]Corresponding author. E-mail: paula.lindgren@geol.lu.se

(Received 14 January 2019; revision accepted 29 July 2019)

Abstract–A carbon-rich melt fragment from the Gardnos impact structure has been studied for a better understanding of the preservation and structural form(s) of carbon that have been processed by impact melting. The carbon was analyzed in situ in its original petrographic context within the melt fragment, using high-resolution techniques including focused ion beam-transmission electron microscopy and electron energy loss spectroscopy. Results show that the carbon is largely uniform and has a nanocrystalline grain size. The Gardnos carbon has a graphitic structure but with a large c/a ratio indicating disorder. The disorder could be a result of rapid heating to high temperatures during impact, followed by rapid cooling, with not enough time to crystallize into highly ordered graphite. However, temperature distribution during impact is extremely heterogenous, and the disordered Gardnos carbon could also represent material that avoided extreme temperatures, and thus, it was preserved. Understanding the structure of carbon during terrestrial impacts is important to help determine if the history of carbon within extraterrestrial samples is impact related. Furthermore, the degree of preservation of carbon during impact is key for locating and detecting organic compounds in extraterrestrial samples. This example from Gardnos, together with previous studies, shows that not all carbon is lost to oxidation during impact but that impact melting can encapsulate and preserve carbon where it is available.

INTRODUCTION

Aim of Study

The behavior of carbonaceous matter during impact shock is poorly understood, and especially the fate of carbon during impact melting. Impacts into carbon-rich targets have long been suggested to cause carbon loss by oxidation to the atmosphere (e.g., Maher and Stevenson 1988; Dypvik et al. 2005). However, in contrast, impact settings with preserved carbon associated with impact melts are detected increasingly more so in the geological record (e.g., Lindgren et al. 2009; Howard et al. 2013; Schultz et al. 2014). In this study, we have used a carbon-rich melt fragment from the Gardnos impact structure in Norway as a natural example to better understand what structural form(s) the carbon takes after incorporation in an impact melt. To achieve this, we used state-of-the-art high-resolution imaging and microanalysis techniques, specifically focused ion beam-transmission electron microscopy (FIB-TEM) and electron energy loss spectroscopy (EELS), to perform a high-resolution in situ study of the Gardnos carbon in

its original petrographic context within a melt fragment in a melt-bearing impact breccia.

Carbon in Impact Structures

Although carbon and organic matter is in general rarely reported at impact sites, terrestrial impact structures are the only geological setting where many polymorphs of carbon have been detected side by side, including graphite, diamond, and fullerenes (Gilmour 1998). The Ries impact structure in Germany is one example of such an impact setting where highly crystalline forms of carbon—graphite and diamond (Hough et al. 1995)—occur together with organic matter that has not been converted into highly crystalline forms of carbon (Hofmann et al. 2001). This reflects the wide range of conditions that occur during impact processes. The Gardnos impactites are highly unusual in that they are 5–10 times enriched in carbon compared to the surrounding bedrock (French et al. 1997; Gilmour et al. 2003). The only other impact structure, recognized so far, with such highly elevated carbon content compared to the surrounding bedrock is the Sudbury impact structure in Canada (Avermann 1994). The carbon in the Gardnos impact structure was most likely sourced from immature organic-rich shale that was included in the target at the time of impact, but is no longer present at the site today, for example, the Proterozoic Biri Shale or the Cambrian Alum Shale (French et al. 1997; Gilmour et al. 2003). Parnell and Lindgren (2006) argued that the most probable shale target was the Alum Shale, as this was the only candidate target rock with adequate amount of carbon. No preserved shale fragments have to our knowledge yet been detected in the Gardnos impact breccias, but shale fragments with kept preimpact carbonaceous matter are previously reported from within the Bunte lithic impact breccia from the Ries impact structure (Hofmann et al. 2001) and fragments of shale are also found in the Loftarsten resurge deposits from the Lockne impact structure in Sweden (Sturkell 1998).

Carbonaceous matter that is particularly associated with melt-bearing impact lithologies is even more unusual, but has nonetheless been reported from a small number of terrestrial impact settings. These include Darwin in Australia (Howard et al. 2013), Sudbury in Canada (Wright et al. 2010), Yanisyarvi (Badjukov and Raitala 1998) and Kara (Korochantsev et al. 2001) in Russia, and Gardnos in Norway (Parnell and Lindgren 2006). Gardnos provides an especially unique opportunity to study carbon–melt interactions, since its melt-bearing impact breccia contain melt fragments that are highly enriched in carbon, with a total organic carbon content of approximately 5% (Parnell and Lindgren 2006).

Geological Setting of the Gardnos Impact Structure

The Gardnos structure is located in the valley of Hallingdal, approximately 9 km north of the small village Nesbyen in southern Norway (Fig. 1). The impact structure is eroded due to Caledonian orogenic uplift and several Pleistocene glaciations. Today the structure is approximately circular with a diameter of approximately 5 km, but the original crater diameter is estimated to have been close to 6 km (Kalleson et al. 2008). It is a complex impact structure and the present structure has a centrally uplifted area of fractured basement rocks that is approximately 0.5 km across (French et al. 1997). The impact has been dated to 546 ± 5 Ma using U-Pb systematics of zircon (Kalleson et al. 2009). The target rocks at Gardnos comprise a Proterozoic metamorphic basement of mostly granites and granitic gneisses, with lesser amounts of quartzite and amphibolites (Fig. 1). These rocks were deformed and metamorphosed in amphibolite facies approximately 1500–1700 Ma ago (Starmer 1991). The crystalline basement was later intruded by pegmatites at 900 Ma ago during the Sveconorwegian Orogeny (Starmer 1993). The pegmatites are regionally relatively undeformed, but at Gardnos, they were deformed during the formation of the impact crater (French et al. 1997). The Caledonian Orogeny was active in the region around 380–400 Ma ago, and has resulted in further deformation and metamorphism of the Gardnos area (French et al. 1997). The metamorphic grade in the Gardnos area during the Caledonian Orogeny reached greenschist facies, which was not strong enough to erase primary features of postimpact infill such as bedding, or to erase shock effects such as planar deformation features in quartz grains of the impact breccias (French et al. 1997).

The Gardnos impactites are composed of both shock-deformed but still coherent basement rocks, for example, a highly fractured shocked quartzite, in addition to lithic- and melt-bearing breccias (Dons and Naterstad 1992; French et al. 1997; Kalleson et al. 2010). The lithic breccias at Gardnos are known as the Gardnos Breccia and the Black-Matrix Breccia. The Gardnos Breccia is composed of approximately 1–2 cm angular fragments of basement rocks, mainly light colored granitic gneisses set in a fine-grained and black lithic matrix. The Black-Matrix Breccia resembles the Gardnos Breccia, but contains lesser amounts and smaller sized, generally <0.5 cm, crystalline rock fragments, set in a very fine and black lithic matrix. The

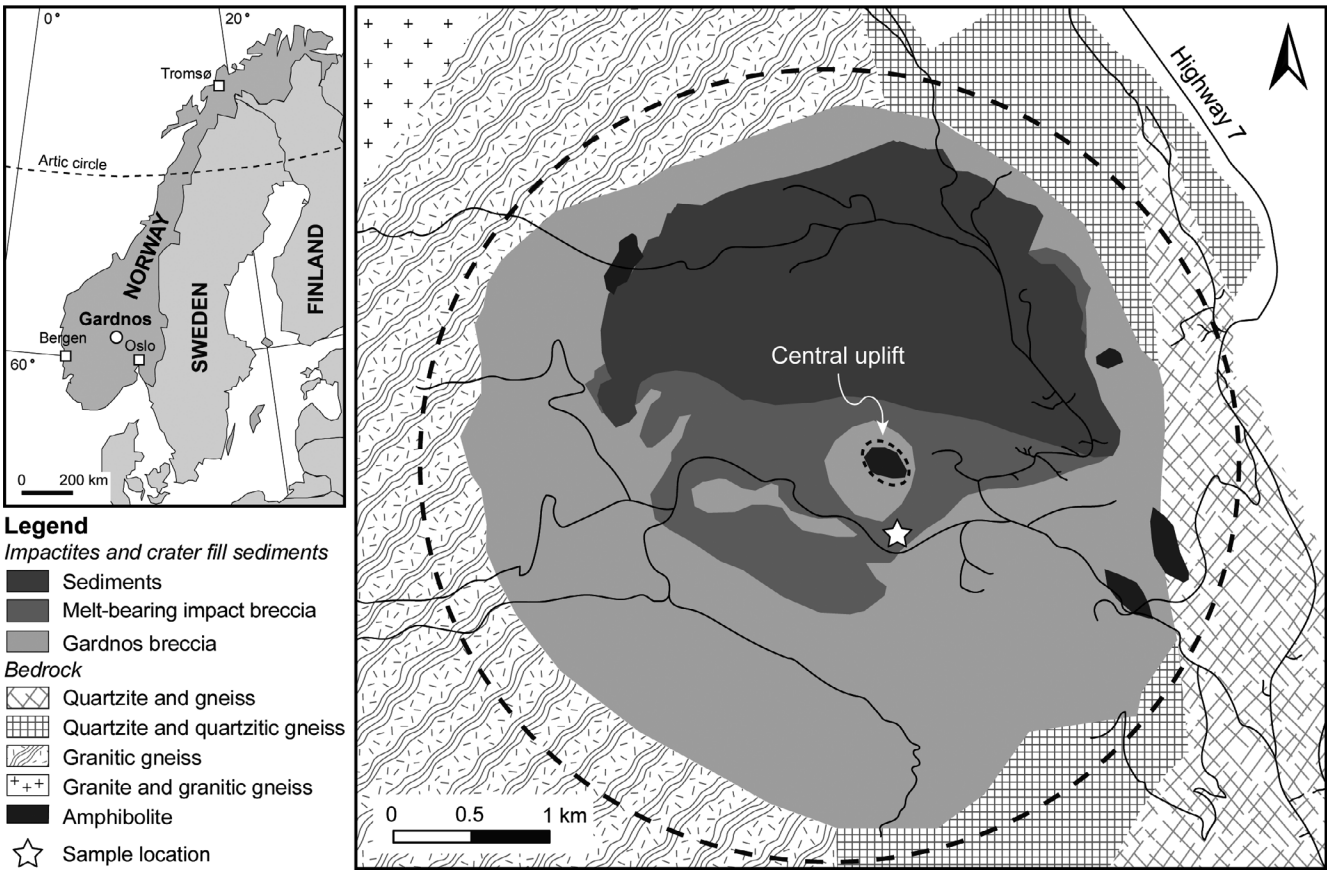

Fig. 1. Geological map of the Gardnos impact structure modified after Kalleson et al. (2008). The map shows target rocks, impactites, the crater rim, and the central uplift. The sample location of melt-bearing impact breccia is marked with a star. The insert map of Scandinavia and Finland marks the location of the Gardnos impact structure approximately 100 km northwest of Oslo in Norway.

lithic breccias are autochthonous brecciated basement; the top of the lithic breccias forms the crater floor (French et al. 1997). The melt-bearing breccias are crater-fill material, and contain both lithic and melt components. They have previously been divided into "suevite" and "melt-matrix breccia" or "clast-rich impact melt." The melt breccias are, however, exceedingly dominated by the "suevite" (French et al. 1997; Gilmour et al. 2003; Kalleson et al. 2010) and this unit is composed of discrete black melt fragments, partially melted crystalline fragments, and lithic fragments, set in a greenish and fine lithic matrix. The "melt-matrix breccia"/"clast-rich impact melt" occurs as lenses within the "suevite" body and is composed of minor amounts of rock and mineral fragments set in a matrix of recrystallized melt (French et al. 1997).

Carbon in Gardnos Impactites

All of the Gardnos impactites contain elevated amounts of carbon and these unusual carbon-bearing breccias were first described by Broch (1945). Broch (1945) initially explained the occurrence of carbon in these rocks as derived from carbon-rich volcanic gases, but later findings of planar deformation features in quartz confirmed an impact origin for Gardnos (Dons and Naterstad 1992). The isotopic composition of the carbon in the Gardnos impactites has a value of −28 to −32 $\delta^{13}C$ consistent with biogenic carbon, as derived from carbon-rich shale, rather than carbon derived from the crystalline basement or from the impactor (French et al. 1997). The Gardnos "suevite" has the highest carbon content of all the impactites at Gardnos, and the carbon here is located within dark melt fragments that have a total organic carbon concentration of around 5% (Parnell and Lindgren 2006). Gilmour et al. (2003) used Raman spectroscopy and transmission electron microscopy to analyze carbon in acid-resistant residues of powdered whole-rock samples from Gardnos. They found poorly ordered carbon, as well as crystalline graphite and microdiamond. Poorly ordered carbon and graphite were detected in both lithic- and melt-bearing

breccias, whereas the microdiamond was detected only in the melt-bearing breccia. Elsila et al. (2005) detected low concentrations of fullerenes at Gardnos, also in acid-resistant residues of powdered samples of both lithic- and melt-bearing impact breccias. Parnell and Lindgren (2006) detected carbon with a low degree of structural order using Raman spectroscopy on thin sections of "suevite." The carbon in the Gardnos impactites have been subjected to previous studies as outlined above, and the Raman spectral analyses in Parnell and Lindgren (2006) were the first and only previous in situ study of the carbon at Gardnos. Parnell and Lindgren (2006) had considered the Gardnos carbon in a petrographic context, but did not image and analyze the carbon nanostructure in high resolution, such as we present in this paper by using state-of-the-art transmission electron microscopy techniques. Knowing the petrographic setting and structure of carbon processed by impact melting will give important insights to the history of carbon in extraterrestrial samples, for example, carbon in lunar samples (Steele et al. 2010), Martian meteorites (Steele et al. 2012a, 2012b), and carbonaceous chondrites (Martins et al. 2013). Likewise, detailed information about the preservation and context of carbon postimpact is crucial for the detection of organic molecules in extraterrestrial samples and during planetary exploration (e.g., Lindgren et al. 2009).

MATERIALS AND METHODS

Samples

The Gardnos impact structure is easily accessible, but exposures are limited due to a cover of glacial moraine. The contact between the lithic- and melt-bearing breccias can be viewed in outcrops of the Dokkelvi River bed, but these outcrops are protected as they are located inside a nature park. Thus, samples of melt-bearing breccia were collected from material excavated during the building of a museum in 2006 (Fig. 1). Our samples of melt-bearing impact breccia at Gardnos consist of what has previously been referred to as "suevite" and is composed of a variety of melt fragments, partially melted crystalline fragments, and lithic crystalline fragments, set in a finely crushed lithic matrix of crystalline material. The proportion of matrix and the different types of fragments vary extensively throughout the "suevite," but field observations by Kalleson et al. (2010) indicate that the melt content averages to approximately 13 vol% in the "suevite" (excluding the clast-rich impact melt) and lithic fragments form approximately 20 vol% of this rock unit as deduced from field observations. The carbon in this lithology occurs within abundant irregularly formed dark melt fragments that range in size from a few millimeters to several centimeters (Parnell and Lindgren 2006; Figs. 2a and 2b). We have imaged and analyzed over 40 such carbon-rich melt fragments using scanning electron microscopy, and they all show the same textures and petrographic context (see below). A high-resolution in situ microanalysis was then for the purpose of this study conducted on one of these fragments (Figs. 2d–f).

Scanning and Transmission Electron Microscopy

Backscattered electron and secondary electron imaging, and energy-dispersive X-ray (EDX) analysis of the selected Gardnos melt fragment were undertaken using a field emission Zeiss Sigma scanning electron microscope (SEM), equipped with an Aztec Oxford microanalysis system at the Imaging Spectroscopy and Analysis Centre, University of Glasgow. The SEM was operated under high vacuum using an acceleration voltage of 20 kV. The EDX detector area was 80 mm^2. X-ray maps with a resolution of ~300 nm/pixel were acquired over a period of ~30 min using a beam current of 3 nA.

Transmission electron microscopy work and associated sample preparation were undertaken at the Kelvin Nanocharacterisation Centre (KNC), University of Glasgow. Three electron-transparent foils (A, B, and C; Fig. 2f) of carbon in the Gardnos melt fragment were prepared using a FEI Nova Nanolab 200 DualBeam FIB instrument equipped with an field-emission electron gun and a Ga^+ ion gun. The foils were lifted out following the procedure of Lee et al. (2003) using 30 kV Ga^+ ions at a range of beam currents. The foils were milled to a thickness of ~1 μm, extracted using an in situ micromanipulator, welded to the tines of a copper holder using electron- and ion-deposited platinum, and finally milled to a thickness of ~100 nm (50 nm in the thinnest areas). Diffraction contrast images and selected area electron diffraction (SAED) patterns were obtained using a FEI Tecnai G^220 TEM operated at 200 kV. A broad beam was used at all times to minimize any beam damage, and no evidence was seen of any beam-induced changes to the sample during observations.

Electron Energy Loss Spectroscopy

Electron energy loss spectroscopy (EELS) standards of highly ordered pyrolytic graphite (HOPG) from Agar Scientific and a fullerene C_{60} sample from Sigma-Aldrich were prepared by dispersion of the materials in 2-propanol and dropping a single drop onto a lacey

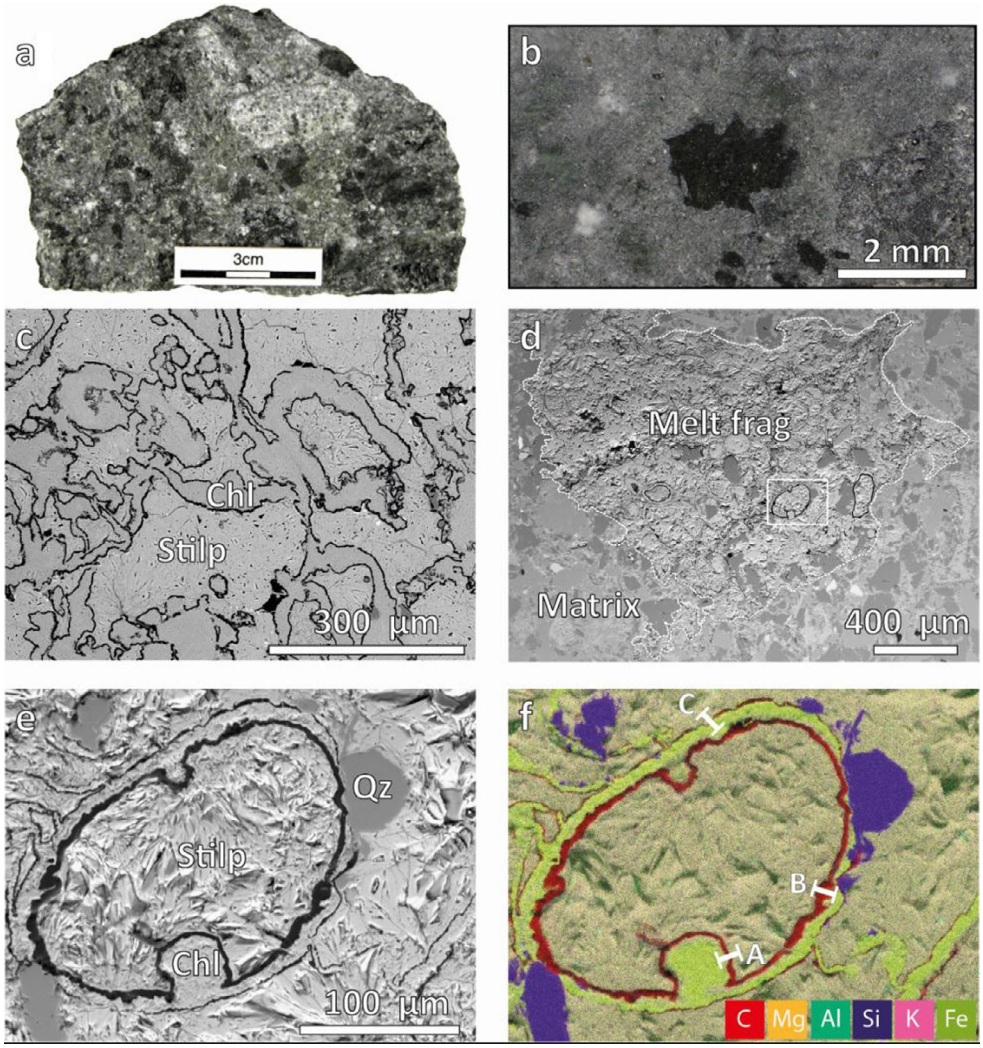

Fig. 2. Hand samples of the Gardnos melt-bearing breccia (a–b) with (a) black carbon-rich melt fragments and crystalline fragments set in a lithic fine-grained matrix, and (b) polished surface showing close-up of a black carbon-rich melt fragment. Scanning electron microscope-backscattered electron micrographs (c–e) and a false colored X-ray map (f) of carbon-rich melt fragments; (c) immiscibility textures of intermingling tunnels inside a melt fragment. Carbon is black highlighting the boundary between chlorite (Chl) and stilpnomelane (Stilp), (d) the melt fragment used in this study. The irregular boundary between the melt fragment and the surrounding matrix is marked with a dotted line, (e) close-up of the area inside the melt fragment marked with a rectangle in (d), showing carbon in black at the boundary between stilpnomelane and chlorite. Quartz (Qz) is also present, (f) false colored X-ray map of (e) showing carbon in red and the location of the three focused ion beam sections (A, B, C). (Color figure can be viewed at wileyonlinelibrary.com.)

carbon support film. The lacey carbon support film itself was also used as a standard for amorphous evaporated carbon. Electron energy loss spectroscopy was performed on the three foils of Gardnos carbon at KNC in Dual EELS acquisition mode with a Gatan GIF Quantum ER mounted on a JEOL ARM200cF. The instrument was operated at 80 kV in TEM convergent beam diffraction mode and with a camera length of 50 cm. Care was taken to spread the beam over a larger sample area, using a weaker condenser lens setting, to reduce intensity and minimize beam damage. No evidence was seen of any beam-induced changes to the material after spectra were recorded. The convergence semiangle of the probe was 2.61 mrad. The spectrometer was operated with a dispersion of 0.025 eV/channel and a high loss energy shift in DualEELS of 270 eV; the full width at half maximum of the zero loss peak was measured as 0.53 eV under these conditions. Using a spectrometer entrance aperture of 5 mm gave a collection semiangle of 2.81 mrad. Summing the convergence and collection semiangles in quadrature (Ahn and Krivanek 1983;

Daniels et al. 2007) gave an effective collection semiangle of 3.84 mrad. This compares to an expected "Magic" collection semiangle of $2q_E$ (Daniels et al. 2007) of 3.81 mrad for 80 kV, which ideally averages out the orientation dependence of the relative main π* and σ* peak contributions to the C *K* ionization edge EEL spectrum of anisotropic carbons, thus resulting in orientationally invariant spectra from graphite and graphitic carbons. While some variations were seen in the relative intensities of π* and σ* peaks for different graphite particles of the HOPG reference sample, the same overall shape was seen in all cases, and a representative spectrum was chosen for comparison to the experimental spectra from the Gardnos carbon. In all cases, a background was fitted before the C *K* edge (using a power-law function) and the background subtracted, prior to Fourier-ratio deconvolution using the simultaneously acquired low loss spectrum to remove the effects of plural scattering.

Electron Microprobe Analyses

Electron microprobe analyses of the silicate phases in the melt fragment were carried out at the University of Aberdeen with an EDX analyzer in a MICROSCAN MK5 electron microprobe from Cambridge Scientific Instruments Ltd. The system used for analyses was a Link Analytical AN10/25S EDX spectrometer. Analyses were acquired and processed with Link's ZAF4/FLS program. The beam size during analyses was 5 μm. The acceleration voltage was set to 15 keV and the beam current was held at 3.0 nA. The standards used were Na (jadeite), Mg (MgO), Al (Al_2O_3), Si (wollastonite), K (K-feldspar), Ca (wollastonite), Ti (TiO_2), Mn (Mn metal), and Fe (Fe metal). The minimum detection limits in oxide wt% were Na_2O (0.21), MgO (0.27), Al_2O_3 (0.29), SiO_2 (0.37), K_2O (0.1), CaO (0.09), TiO_2 (0.14), MnO (0.21), and FeO (0.59).

RESULTS AND DISCUSSION

Petrographic Context and Origin of the Gardnos Carbon

This study focuses on carbon within melt-bearing breccia from Gardnos. The relevant melt-bearing breccia, in previous publications referred to as "suevite" (e.g., French et al. 1997; Gilmour et al. 2003; Kalleson et al. 2010), is composed of discrete dark melt fragments, partially melted crystalline fragments, and lithic fragments, set in a fine-grained lithic matrix. Here, the carbon is localized exclusively within the dark melt fragments (Figs. 2a–f; Parnell and Lindgren 2006). The dark melt fragments are irregular in shape and millimeters to centimeters in size. They are composed mainly of the two silicates, chlorite and stilpnomelane (Figs. 2a–f; Table 1). Furthermore, quartz is present in the stilpnomelane phase, and crystals of titanite occur within the chlorite phase—indicating that its precursor melt was enriched in titanium. Chlorite and stilpnomelane are typical secondary minerals, but likely still reflect the composition of the precursor melt phases. The carbon occurs as a 2.4 ± 1.2 μm (n = 200) thick film at the boundary between the stilpnomelane and chlorite, and between the stilpnomelane and the matrix, but never between the chlorite and the matrix. The carbon film highlights the textures of melt immiscibility and flow (Figs. 2c–f; Lindgren and Parnell 2005).

The Gardnos carbon was most likely incorporated in the melt when an organic-rich shale target (Alum Shale or Biri Shale), no longer present at the site, was melted. The carbon subsequently precipitated within the stilpnomelane phase, explaining why it never occurs between the chlorite phase and the matrix (Parnell and Lindgren 2006). The stilpnomelane phase is enriched in Si (~48 oxide%) and K (~1.9 oxide%) compared to the chlorite phase (~27 oxide% Si and ~0.2 oxide% K; Table 1). Carbon precipitation from the potassium-enriched stilpnomelane phase is consistent with evidence from diamond chemistry where carbon originates from the alkali-rich component of immiscible mantle-derived liquids (Korsakov et al. 2004). Liquid immiscibility between two silicates in a melt-bearing impact breccia has also been reported from, for example, the Ries impact structure where one of the immiscible phases is, similar to Gardnos, enriched in Si and K and depleted in Ti, compared to the other phase (Osinski 2004).

Micro- and Nanostructure of the Gardnos Carbon

The FIB sections for TEM and EELS analyses (A, B, and C in Fig. 2f) all showed similar features that are described below. Figure 3 highlights the TEM analyses of Section B. It shows a low magnification dark field TEM image of the carbon at the carbon-stilpnomelane boundary (Fig. 3a), with the dark field tilts set in order to place part of the graphitic diffraction ring (0002) into the objective aperture (Fig. 3b inset). The bright contrast of the carbon in (0002) dark field images (e.g., Fig. 3a) shows that the carbon has a nanocrystalline structure with a significant graphitic character. This finding is consistent with the fact that SAED patterns of the carbon comprise broad diffuse rings in the approximate positions of the three strongest reflections for graphite (Fig. 3b inset). This pattern was radially integrated to the line trace of Fig. 3b, and a background-subtracted version of the trace is portrayed to show the peak positions corresponding to the three rings. The best match for the ratio of the $(10\bar{1}1)$ and

Table 1. Compositions of the two main silicate phases occurring with the carbon in a dark melt fragment from Gardnos (wt% oxide).

Phase	Na_2O	MgO	Al_2O_3	SiO_2	K_2O	CaO	TiO_2	MnO	FeO	Total
Stilpnomelane-1	0.98	7.31	6.10	47.72	2.02	b.d.	b.d.	1.18	28.24	93.55
Stilpnomelane-2	0.56	7.55	6.22	48.72	1.73	0.09	b.d.	1.10	28.38	94.35
Chlorite-1	0.42	12.74	16.49	27.56	0.21	b.d.	b.d.	0.46	26.47	84.35
Chlorite-2	b.d.	14.10	18.87	26.91	b.d.	b.d.	b.d.	0.43	28.61	88.92

b.d., below detection limit.

(0002) ring radii is for a c/a ratio of 2.83. For a well-ordered graphite, like that recorded by Trucano and Chen (1975), c/a is somewhat lower, about 2.72. Gamlen and White (1976) found a larger c/a of 2.79 in a more disordered carbon black (formed during the incomplete combustion of heavy petroleum) with lattice parameters of $a = 2.47$ Å and $c = 6.9$ Å, and they referred to this as "graphon." In our case, if we assume that the a-parameter is not strongly affected by disorder, the main changes are likely to be graphite sheet spacings, and thus represented by the c-parameter. C–C bonds in the rings should probably not change much in spacing, although note that Daniels et al. (2007) showed a small change in a-parameters upon graphitization during heat treatment of petroleum pitch. Consequently, we could estimate $c = 7$ Å assuming $a = 2.47$ Å, which is even higher than in the "graphon" of Gamlen and White (1976). It should, however, be noted that this parameter is an average of a distribution of parameters. Both the $(10\bar{1}1)$ and (0002) rings are broad and they cover a range of angles, which is likely because the crystallite size is small and therefore resulting in a large amount of Scherrer broadening of diffraction peaks (Patterson 1939). However, the asymmetry of the two peaks (Fig. 3b) would suggest that this is not the only effect and that there is plenty of structural disorder and a range of lattice spacings present, possibly affecting both the a and c axis parameters. Gamlen and White (1976), Kovalevski et al. (2001), and Zhang et al. (2011) also noted similar broad, asymmetric diffraction maxima. The high c-parameter in the Gardnos carbon could suggest intercalation of other atoms in-between layers, possibly because of incomplete conversion of hydrocarbons in the target shale into graphitic carbon (as is a well-known phenomenon in soot, carbon black, and coal). Support for this view is found in the work of Oberlin (1984), in which the c-parameter determined from X-ray diffraction of coal tar pitch reduced with the increasing temperature of a graphitization heat treatment. This would suggest a gradual driving out of the intercalated atoms between the sheets, a collapse of the c-parameter toward the value for well-ordered graphite, and a reduction in disorder, all because of annealing. In addition, recent work at high pressure in a diamond anvil cell suggests that H_2 dimers can intercalate between layers in graphite (Lim and Yoo 2016), increasing the layer spacing, giving further support to the idea that intercalated atoms may cause the c-spacing increase observed by ourselves and others in disordered nanocrystalline graphitic materials.

Higher magnification 0002 dark field images are shown in Figs. 3c–d. In Fig. 3c, a part of the ring away from the bright spot circled in Fig. 3b was used, whereas in Fig. 3d, the circled part of the ring was used. Thus, Figs. 3c–d show graphitic areas with a different relative orientation of their respective basal planes, and upon closer inspection, both figures show bright speckles 1–3 nm in size. These are individual diffracting crystallites. In the case of Fig. 3d, however, many speckles are arranged in an area of similar orientation, that is also seen as the longer linear feature in the lower left of Fig. 3a. There are three similar linear features on the right-hand side of Fig. 3a, and it seems at first that these are larger flakes of graphite with some preferred orientation. However, the dominance of nanosized crystallites within this carbon, as shown by the nanoscale speckles (Fig. 3d), indicates it is unlikely these linear features are single crystal flakes with a perfect orientation.

The EEL spectra (Fig. 4) show the C K-edge from the Gardnos carbon in two FIB sections (B and C in Fig. 2f). These are compared to the EEL spectra from a HOPG graphite standard, a C_{60} fullerene standard, and evaporated amorphous carbon. The HOPG graphite spectrum represents a well-ordered sample with millimeter-sized graphite flakes. The C_{60} fullerene represents carbon containing a large amount of six-membered rings, but with a significant population of five-membered rings. Finally, the amorphous C-film represents a more disordered carbon. Clearly, the Gardnos carbon most closely approximates to the graphite spectrum, demonstrating that the Gardnos carbon is substantially graphitic in character. Nevertheless, a detailed comparison of the HOPG graphite and the Gardnos spectra reveals a key difference; in the HOPG graphite, the "valley" between the π^* and σ^* peaks of the C K-edge is almost flat and

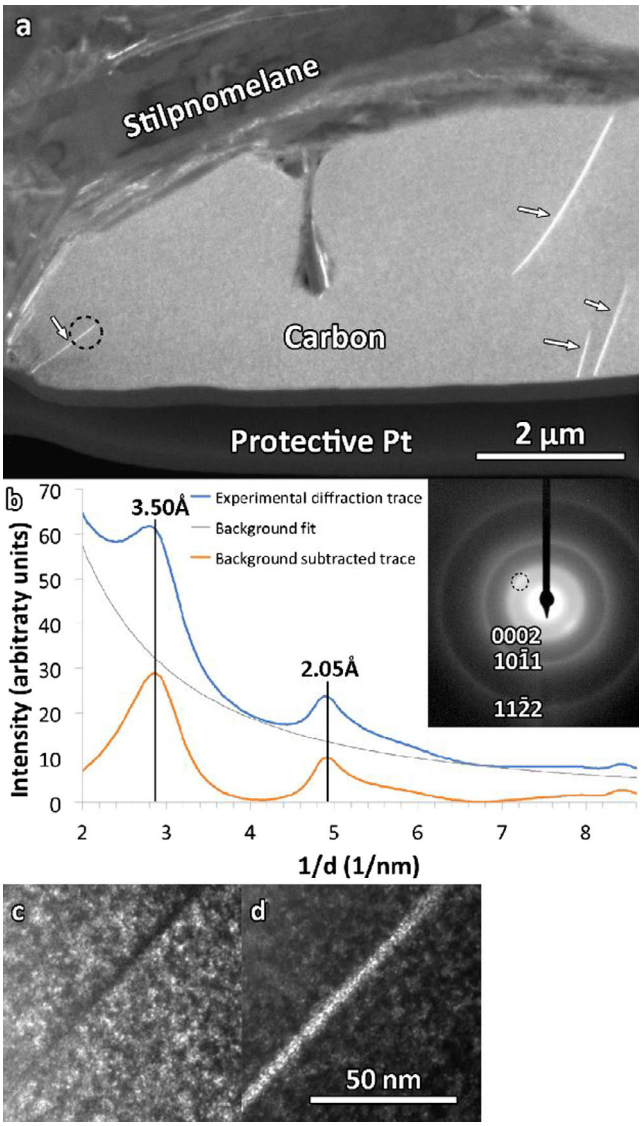

Fig. 3. Transmission electron microscopy studies of a focused ion beam section of the Gardnos carbon (Section B in Fig. 2f). a) Dark field image from a diffracted angle corresponding to the 0002 ring for graphite, arrows are pointing to bright linear features in the carbon; (b) radial integration of diffraction trace with inset of selected area diffraction pattern of an area marked by a circle in (a). The circle in (b) highlights a brighter spot on the 0002 ring that is perpendicular to the linear feature in (a); (c) higher magnification 0002 dark field image of a region containing the linear feature encircled in (a), with the dark field tilt set to emphasize the microstructure of the surrounding carbon; (d) 0002 dark field image of the exact same area as in (c), but with the dark field tilt set so that the ringed area of the diffraction pattern in (b) is the area selected by the objective aperture. (Color figure can be viewed at wileyonlinelibrary.com.)

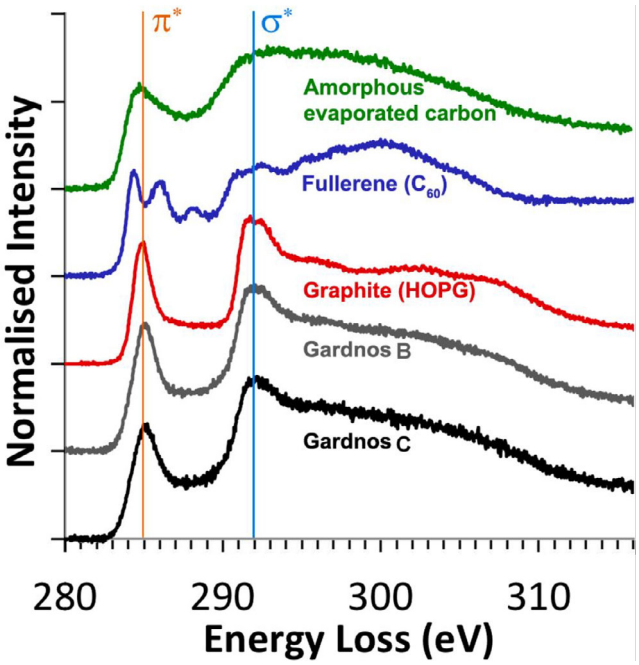

Fig. 4. Electron energy loss spectra of the Gardnos carbon in two focused ion beam sections (Sections B and C in Fig. 2f), compared to a highly ordered pyrolytic graphite standard, C_{60} fullerene standard and an amorphous carbon film. All spectra have been Fourier-ratio deconvolved to remove the effects of plural scattering. (Color figure can be viewed at wileyonlinelibrary.com.)

dropping slightly toward the σ* peak, but in the Gardnos samples, this "valley" is not quite as deep and not flat at the bottom. The variation in this "valley intensity" between the π* and σ* peaks is due to an increase of disorder of the Gardnos carbon, that is, a deviation from a perfect C–C sp^2 bonding (Suenaga and Koshino 2010; Kepaptsoglou et al. 2015). In fact, the shape of this "valley" and peak arrangement is rather similar to that seen in EELS edges of graphitic carbons created by heat treatment of phenolic resin at 2000 °C or 2500 °C (particularly fig. 7 of Zhang et al. 2011). Albeit having a predominantly graphitic character, the disorder seen in the Gardnos carbon could be a result of an unusual mode of formation comprising instantaneous heating to extremely high temperatures during impact, followed by a rapid cooling with not enough time to crystallize into highly ordered graphite. The presence of nanosized crystallites, rather than larger crystals, also supports such rapid cooling. Disordering is further in agreement with the strong D (disordered) peak present within the Raman spectra of Gardnos carbon (at 1350 cm^{-1}; Parnell and Lindgren 2006). Finally, the similarity of both the diffraction patterns and the EELS edges seen in this study, compared to those seen previously for heat-treated hydrocarbons, would suggest that heating to high temperatures of at least 2000 °C in oxygen-poor conditions was the probable mode of formation of the Gardnos carbon. However, there are also other scenarios

to explain the disordered graphite in the Gardnos melt. There are, for example, many cases of disordered graphite in metamorphic rocks where despite a lengthy time span with high temperature and pressure, this has still not been enough to cause highly ordered graphite (Papineau et al. 2009, 2019). Temperature distribution during impact can be extremely heterogeneous and although the carbon at Gardnos resides in the high-temperature melt breccias, it could represent material that avoided extreme temperature and that is then the reason it is preserved. In this case, the disordered nanocrystalline graphite would reflect heating being insufficient to cause highly ordered graphite. Another possibility is that the carbon in the melts is later stage and related to hydrothermal processes in the postimpact environment. This is a detailed, but yet limited, study of carbon in one melt fragment, and it is possible that if more samples were analyzed, one could expect a variation in ordering reflecting the heterogeneity of shock. Here, we studied carbon in a melt fragment in the "suevite," but carbon and organic matter also occur in the other impactites at Gardnos (e.g., French et al. 1997; Gilmour et al. 2003).

Implications for the Preservation and Detection of Carbon in Extraterrestrial Samples

The disequilibrium and the wide range of conditions during impacts are reflected in that, for example, shocked quartz can occur together with unshocked quartz, diaplectic glass, and silicate melts, and that many polymorphs of carbon can occur together (Gilmour 1998). In this study, we have specifically focused on carbon during one of these impact conditions, namely carbon processed by impact melting. The behavior of carbon during impact melting is not well understood, and it has been suggested that impacts into carbon-rich targets causes carbon loss to the atmosphere due to oxidation (Dypvik et al. 2005). The organic-rich shale that is the probable precursor to the Gardnos carbon is not preserved at the impact site; however, the carbon itself is preserved within the impactites. In fact, the melt-bearing breccias have the highest carbon content of all the impactites at Gardnos and the carbon therein is concentrated in the melt fragments. This indicates that a substantial amount of the carbon in the Gardnos impactites was not oxidized, but rather incorporated into the melt. The amount of carbon preserved in the Gardnos melt is estimated to be at least 31% (Parnell and Lindgren 2006).

In addition to Gardnos, there are other natural examples of carbon preserved in terrestrial impact melts, for example, in the Sudbury structure, Canada (Bunch et al. 1999; Wright et al. 2010). At Sudbury, spherules of both graphitic and more disordered carbon are reported within chalcopyrite crystals, suggesting that the carbon there had behaved as a chalcophile element in the impact melt (Wright et al. 2010). The melt-processed Sudbury carbon was characterized using Raman spectroscopy; thus, inspection of the same carbon at a submicron resolution (e.g., via TEM and EELS) may provide a higher level of structural detail. Another example of carbon processed by impact melts comes from the Darwin impact structure in Australia. At Darwin, biomarkers representative of plant species in the local ecosystem at the time of impact, including cellulose, lignin, aliphatic biopolymer, and protein remnants, are preserved in amorphous carbon glasses contained inside silicate impact melt ejecta. The Darwin carbon shows no evidence of graphite, but is amorphous glass as shown by, for example, TEM, and preservation is interpreted to be related to low peak temperatures rather than rapid cooling after extreme heating. Also, Lindgren et al. (2009) and Schultz et al. (2014) found organic biomarkers preserved in impact melt breccias. The former was within lithic clasts in a melt breccia, so not directly in the impact melt itself, and the latter from leaf fragments encapsulated within impact melt glass. These examples highlight that carbon associated with other impact melts does not necessarily have the same history as the carbon in the Gardnos impact melts.

Nevertheless, the presence of carbon in the impact melts from, for example, Gardnos, Sudbury, and Darwin, indicates that, while some carbon may be lost to oxidation in a terrestrial setting, not all carbon is lost —even with an oxygen-rich atmosphere. Therefore, it follows that under less oxidizing conditions—for example, at depth under reducing conditions, on airless planetary bodies, or those with oxygen-poor atmospheres—a lower proportion of carbon would be lost via oxidation, and even more would be preserved within the impact melts. Impact melts also bear the evidence of creating a reducing microenvironment, which would favor carbon preservation. For example, the presence of magnetite spherules, native iron, and wüstite indicates strongly reducing conditions during impact melting (Vishnevsky and Raitala 2003). However, there are also many examples of oxidized impact glasses, but then again, alteration overprinting is common in impact settings and it can complicate interpretation of what are primary and secondary phases.

Knowledge of the carbon structure during terrestrial impacts can be used to help determine if carbon within extraterrestrial samples is impact related. Carbon in extraterrestrial settings includes graphitic carbon within a lunar impact melt breccia returned from the Moon by

the Apollo 17 mission (Steele et al. 2010). This breccia is interpreted to have formed via the impact of a carbonaceous chondrite meteorite, where the organic matter in the carbonaceous chondrite impactor was transformed into graphite during impact and then preserved in the resulting impact melt breccia. Carbon is also reported in several Martian meteorites (Steele et al. 2012a), occurring as macromolecular carbon (MMC) inclusions with similar Raman D and G bands to those reported previously from the Gardnos carbon (e.g., Parnell and Lindgren 2006). However, detailed studies, combining in situ Raman spectroscopy with TEM, X-ray absorption near-edge spectroscopy, and bulk-rock carbon analyses revealed the Martian MMC to be dominated by aromatic rings, with C–H and C–O bonds evident (e.g., Steele et al. 2016). The Martian MMC probably originated in the planet's interior, and was erupted and trapped within igneous rocks when they crystallized (Steele et al. 2012b). However, two Martian meteorites (Tissint and ALH 84001) do reportedly contain graphitic carbon (Steele et al. 2012a, 2016). These are among the most heavily shocked Martian meteorites (e.g., Treiman 1998; Baziotis et al. 2013; Walton et al. 2014); hence, their graphitic carbon could have been formed via impact processing of the original MMC (Steele et al. 2012b, 2016).

CONCLUSIONS

Carbon is preserved within melt fragments, composed mainly of stilpnomelane and chlorite, in melt-bearing impact breccia from the Gardnos impact structure. This carbon has a nanocrystalline grain size, so it is not amorphous. It is largely uniform, except for some linear features consisting of numerous crystallites of similar orientation. Electron diffraction shows that the atomic structure of the Gardnos carbon is disordered with a large c/a ratio graphitic structure. Electron energy loss spectroscopy is fully consistent with this finding, displaying C *K*-edge spectra similar to those for HOPG, but with some differences suggesting a significant disorder in the graphite. This could be a consequence of rapid heating to high temperatures during impact, followed by rapid cooling, with insufficient time to crystallize into highly ordered graphite. However, since temperature distribution during impact is extremely heterogenous, the disordered Gardnos carbon could also represent material that was preserved because it avoided extreme temperatures, or the disordered carbon could be related to postimpact hydrothermal processes.

This work showing the fate of carbon during impact melting demonstrates an approach to understanding the structure and formation of impact processed carbon that is also applicable to carbon in extraterrestrial samples. The presence of carbon within Gardnos and other terrestrial impact melts indicates that not all carbon is lost to oxidation during impact events, even within an oxygen-rich atmosphere. Thus, under less oxidizing conditions in extraterrestrial settings, carbon loss from the target via oxidation during impact would decrease and even more carbon would be preserved within impact melts. This example from Gardnos, together with previous studies, shows that impact melting can encapsulate and preserve carbonaceous matter where it is available.

Acknowledgments—We are grateful for grants received from the UK Science and Technology Facilities Council (grant numbers ST/K000942/1 and ST/N000846/1) and the Swedish Research Council (grant number 2015-04084). Philippa Ascough at the Scottish Universities Environmental Research Centre provided the HOPG graphite standard. John Still at the University of Aberdeen performed the electron microprobe analyses and William Smith at the University of Glasgow prepared the TEM samples using the focused ion beam instrument. SuperSTEM is the UK Engineering and Physical Sciences Research Council (EPSRC) National Research Facility for Advanced Electron Microscopy. We are grateful to comments from two reviewers that improved our manuscript.

Editorial Handling—Dr. Gordon Osinski

REFERENCES

Ahn C. C. and Krivanek O. L. 1983. *EELS atlas: A reference guide of electron energy loss spectra covering all stable elements*. Tempe, Arizona: Arizona State University and Gatan Inc..

Avermann M. 1994. Origin of the polymict, allochthonous breccias of the Onaping Formation, Sudbury structure, Canada. In *Large meteorite impacts and planetary evolution* edited by Dressler B. O., Grieve R. A. F., and Sharpton V. L. GSA Special Paper 293. Boulder, Colorado: Geological Society of America. pp. 265–274.

Badjukov D. D. and Raitala J. 1998. The impact melt of the Janisjarvi crater (abstract #1609). 29th Lunar and Planetary Science Conference. CD-ROM.

Baziotis I. P., Liu Y., DeCarli P. S., Melosh H. J., McSween H. Y., Bodnar R. J., and Taylor L. A. 2013. The Tissint Martian meteorite as evidence for the largest impact excavation. *Nature Communications* 4:1404.

Broch O. A. B. 1945. Gardnosbreksjen i Hallingdal. *Norsk Geologisk Tidskrift* 25:16–25.

Bunch T. E., Becker L., Des Marais D., Tharpe A., Schultz P. H., Wolbach W., Glavin D. P., Brinton K. L., and Bada J. L. 1999. Carbonaceous matter in the rocks of the Sudbury Basin, Ontario, Canada. GSA Special Paper 339, edited by Dressler B. O. and Sharpton V. L. Boulder, Colorado: Geological Society of America. pp. 331–343.

Daniels H., Brydson R., and Brown A. 2007. Investigating carbonization and graphitization using electron energy loss spectroscopy (EELS) in the transmission electron microscope (TEM). *Philosophical Magazine* 87:4073–4092.

Dons J. A. and Naterstad J. 1992. The Gardnos impact structure, Norway. *Meteoritics* 27:215.

Dypvik H., Wolbach W. S., Shuvalov V., and Weaver S. L. W. 2005. Did the Mjølnir asteroid impact ignite the Barents Sea hydrocarbon source rocks? (abstract #1020). 36th Lunar and Planetary Science Conference. CD-ROM.

Elsila J. E., De Leon N. P., Plows F. L., Buseck P. R., and Zare R. N. 2005. Extracts of impact breccia samples from Sudbury, Gardnos and Ries impact craters and the effects of aggregation on C_{60} detection. *Geochimica et Cosmochimica Acta* 69:2891–2899.

French B. M., Koeberl C., Gilmour I., Shirey S. B., Dons J. A., and Naterstad J. 1997. The Gardnos impact structure, Norway: Petrology and geochemistry of target rocks and impactites. *Geochimica et Cosmochimica Acta* 61:873–904.

Gamlen P. H. and White D. J. 1976. Structure and dynamics of microcrystalline graphite, graphon, by neutron scattering. *Journal of the Chemical Society, Faraday Transactions 2: Molecular and Chemical Physics* 72:446–455.

Gilmour I. 1998. Geochemistry of carbon in terrestrial impact processes. In *Meteorites: Flux with time and impact effects*, edited by Grady M. M., Hutchison R., McCall G. J. H., and Rothery D. A. Special Publication 140. London: Geological Society of London. pp. 205–216.

Gilmour I., French B. M., Franchi I. A., Abbott J. I., Hough R. M., Newton J., and Koeberl C. 2003. Geochemistry of carbonaceous impactites from the Gardnos impact structure, Norway. *Geochimica et Cosmochimica Acta* 67:3889–3903.

Hofmann P., Leythaeuser D., and Schwark L. 2001. Organic matter from the Bunte Breccia of the Ries Crater, southern Germany: Investigating possible thermal effects of the impact. *Planetary and Space Science* 49:845–851.

Hough R. M., Gilmour I., Pillinger C. T., Arden J. W., Gilkess K. W. R., Yuan J., and Milledge H. J. 1995. Diamond and silicon-carbide in impact melt-rock from the Ries impact crater. *Nature* 378:41–44.

Howard K. T., Bailey M. J., Berhanu D., Bland P. A., Cressey G., Howard L. E., Jeynes C., Matthewman R., Martins Z., Sephton M. A., Stolojan V., and Verchovsky S. 2013. Biomass preservation in impact melt ejecta. *Nature Geoscience* 6:1018–1022.

Kalleson E., Dypvik D., and Naterstad J. 2008. Post-impact sediments in the Gardnos impact structure, Norway. In *The sedimentary record of meteorite impacts*, edited by Evans K., Horton D. T. Jr., and Morrow J. R. GSA Special Paper 437. Boulder, Colorado: Geological Society of America. pp. 19–41.

Kalleson E., Corfu F., and Dypvik H. 2009. U-Pb systematics of zircon and titanite from the Gardnos impact structure, Norway: Evidence for impact at 546 Ma? *Geochimica et Cosmochimica Acta* 73:3077–3092.

Kalleson E., Dypvik H., and Nilsen O. 2010. Melt-bearing impactites (suevite and impact melt rock) within the Gardnos structure, Norway. *Meteoritics & Planetary Science* 45:798–827.

Kepaptsoglou D., Hardcastle T. P., Seabourne C. R., Bangert U., Zan R., Amani J. A., Hofsäss H., Nicholls R. J., Brydson R. M. D., Scott A. J., and Ramasse Q. M. 2015. Electronic structure modification of ion implanted graphene: The spectroscopic signatures of p- and n-type doping. *American Chemical Society NANO* 11:11,398–11,207.

Korochantsev A. V., Badjukov D. D., and Sadilenko D. A. 2001. Shock metamorphism of organic matter (abstract #5122). 64th Annual Meteoritical Society Meeting.

Korsakov A. V., Theunisen K., and Smirnova L. V. 2004. Intergranular diamonds derived from partial melting of crustal rocks at ultrahigh-pressure metamorphic conditions. *Terra Nova* 16:146–151.

Kovalevski V. V., Buseck P. R., and Cowley J. M. 2001. Comparison of carbon in shungite rocks to other natural carbons: An X-ray and TEM study. *Carbon* 39:243–256.

Lee M. R., Bland P. A., and Graham G. 2003. Preparation of TEM samples by focused ion beam (FIB) techniques: Applications to the study of clays and phyllosilicates in meteorites. *Mineralogical Magazine* 67:581–592.

Lim J. and Yoo C.-S. 2016. Intercalation of solid hydrogen into graphite under pressures. *Applied Physics Letters* 109:051905.

Lindgren P. and Parnell J. 2005. Liquid immiscibility in suevite melt, Gardnos impact crater (abstract #1629) 36th Lunar and Planetary Science Conference. CD-ROM.

Lindgren P., Parnell J., Bowden S., Taylor C., Osinski G. R., and Lee P. 2009. Preservation of biological markers in clasts within impact melt breccias from the Haughton impact structure, Devon Island. *Astrobiology* 9:391–400.

Maher K. A. and Stevenson D. J. 1988. Impact frustration of the origin of life. *Nature* 331:612–614.

Martins Z., Price M. C., Goldman N., Sephton M. A., and Burchell M. J. 2013. Shock synthesis of amino acids from impacting cometary and icy planet surface analogues. *Nature Geoscience* 6:1045–1049.

Oberlin A. 1984. Carbonization and graphitization. *Carbon* 6:521–541.

Osinski G. R. 2004. The nature of the groundmass of surficial suevite from the Ries impact structure, Germany, and constraints on its origin. *Meteoritics & Planetary Science* 39:1655–1683.

Papineau D., Purohit R., Goldberg T., Pi D., Shields G. A., Bhu H., Steele A., and Fogel M. L. 2009. High primary productivity and nitrogen cycling after the Paleoproterozoic phosphogenic event in the Aravalli Supergroup, India. *Precambrian Research* 171:37–56.

Papineau D., De Gregorio B. T., Sagar J., Thorogate R., Wang J., Nittler L., Kilcoyne D. A., Marbach H., Drost M., and Thornton G. 2019. Fossil biomass preserved as graphitic carbon in a late Paleoproterozoic banded iron formation metamorphosed at more than 550°C. *Journal of the Geological Society* 176:651–668.

Parnell J. and Lindgren P. 2006. Survival of reactive carbon through meteorite impact melting. *Geology* 34:1029–1032.

Patterson A. L. 1939. The scherrer formula for X-Ray particle size determination. *Physical Reviews* 56:978–982.

Schultz P. H., Harris R. S., Clemett S. J., Thomas-Keprta K. L., and Zárate M. 2014. Preserved flora and organics in impact melt breccias. *Geology* 42:515–518.

Starmer I. C. 1991. The Proterozoic evolution of the Bamble sector shear belt, southern Norway: Correlations across southern Scandinavia and the Grenvillian controversy. *Precambrian Research* 49:107–139.

Starmer I. C. 1993. The Sveconorwegian Orogeny in southern Norway, relative to deep crustal structure and events in

the North Atlantic Proterozoic supercontinent. *Norsk Geologisk Tidskrift* 73:109–132.

Steele A., McCubbin F. M., Fries M. D., Glamoclija M., Kater L., and Nekvasil H. 2010. Graphite in an Apollo 17 impact melt breccia. *Science* 329:51.

Steele A., McCubbin F. M., Fries M., Kater L., Boctor N. Z., Fogel M. L., Conrad P. G., Glamoclija M., Spencer M., Morrow A. L., and Hammond M. R. 2012a. A reduced organic carbon content in Martian basalts. *Science* 337:212–215.

Steele A., McCubbin F. M., Fries M. D., Golden D. C., Ming D. W., and Benning L. G. 2012b. Graphite in the Martian meteorite Allan Hills 84001. *American Mineralogist* 97:1256–1259.

Steele A., McCubbin F. M., and Fries M. D. 2016. The provenance, formation, and implications of reduced carbon phases in Martian meteorites. *Meteoritics & Planetary Science* 51:2203–2225.

Sturkell E. F. F. 1998. The marine Lockne impact structure, Jämtland, Sweden: A review. *Geologische Rundschau* 87:253–267.

Suenaga K. and Koshino M. 2010. Atom-by-atom spectroscopy at graphene edge. *Nature* 468:1088–1090.

Treiman A. H. 1998. The history of Allan Hills 84001 revised: Multiple shock events. *Meteoritics & Planetary Science* 33:753–764.

Trucano P. and Chen R. 1975. Structure of graphite by neutron diffraction. *Nature* 258:136–137.

Vishnevsky S. A. and Raitala J. 2003. Native iron, wüstite and magnetite in impactites of Janisjärvi and Gardnos crater (The Baltic shield) (abstract #5072). 66th Annual Meeting of the Meteoritical Society.

Walton E. L., Sharp T. G., Hu J., and Filiberto J. 2014. Heterogeneous mineral assemblages in Martian meteorite Tissint as a result of a recent small impact event on Mars. *Geochimica et Cosmochimica Acta* 140:334–348.

Wright A. J., Parnell J., and Ames D. E. 2010. Carbon spherules in Ni-Cu-PGE sulphide deposits in the Sudbury impact structure, Canada. *Precambrian Research* 177:23–38.

Zhang Z., Brydson R., Aslam Z., Reddy S., Brown A., Westwood A., and Rand B. 2011. Investigating the structure of non-graphitising carbons using electron energy loss spectroscopy in the transmission electron microscope. *Carbon* 49:5049–5063.